Volume 17
Number 21
2 June 2026
Pages 2147-2276

Polymer Chemistry

rsc.li/polymers

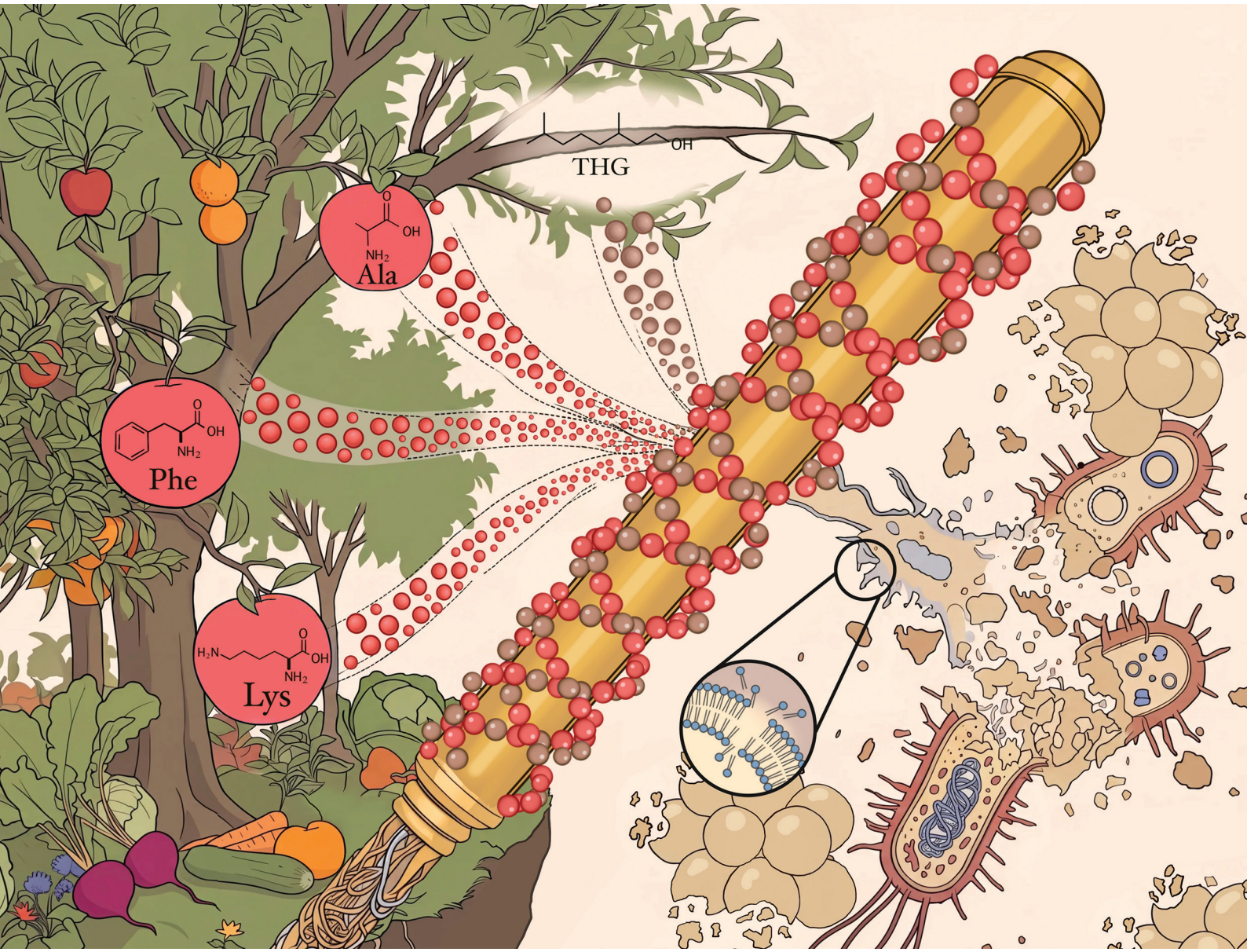

ISSN 1759-9962

ROYAL SOCIETY OF CHEMISTRY

PAPER

Patrizio Raffa *et al.*

Antimicrobial amphiphilic random copolymers from bio-based methacrylates: effect of chemical composition on activity and selectivity

Polymer Chemistry

ROYAL SOCIETY OF CHEMISTRY

PAPER

View Article Online
View Journal | View Issue

Check for updates

Cite this: *Polym. Chem.*, 2026, **17**, 2153

Antimicrobial amphiphilic random copolymers from bio-based methacrylates: effect of chemical composition on activity and selectivity

Zao Cheng, [a,b] Erika Zaganelli, [a,d] Theo van Kooten,[b] Caterina Presutti,[c] Bert Poolman,[c] Laura Mazzocchetti [d] and Patrizio Raffa *[a]

Antibiotic resistance is a growing global threat, prompting the development of novel synthetic antimicrobial agents. Many systems are inspired by antimicrobial peptides (AMPs), which are structurally cationic amphiphilic copolymers. To mimic this type of structure, using at the same time bio-based building blocks, in this study, we synthesized 15 amphiphilic random copolymers using amino acid-derived methacrylates with different side chains (Ala, Phe, and Lys) as the cationic components and bio-based tetrahydrogeranyl methacrylate (THGA) as the hydrophobic component *via* Reversible Addition–Fragmentation chain Transfer (RAFT) polymerization, yielding copolymers with varied cationic–hydrophobic balances. The antimicrobial activity of these copolymers was evaluated against *E. coli* and *S. aureus*, whereas cytotoxicity was evaluated using mouse fibroblasts (*L*929). The results indicate that Lys-based copolymers with higher cationic content are the most active and selective. Activity against *S. aureus* was influenced by the hydrophobic–hydrophilic balance, showing a non-linear trend. The cytotoxicity of these polymers also increased with the rise in cationic content. Live/dead staining, SEM, and calcein leakage assays confirmed the membrane-disrupting effects of random copolymers containing Lys as the cationic component. Furthermore, leakage was observed in liposomes mimicking bacterial membranes at concentrations below the minimum inhibitory concentration (MIC). These findings highlight the potential of bio-based amphiphilic copolymers as selective antimicrobial agents, paving the way for a more sustainable design of such pharmaceutical products.

Received 26th March 2026,
Accepted 21st April 2026

DOI: 10.1039/d6py00298f

rsc.li/polymers

Open Access Article. Published on 22 april 2026. Downloaded on 03.06.2026 13:44:47.
This article is licensed under a Creative Commons Attribution 3.0 Unported Licence.

1. Introduction

Controlling the proliferation of harmful microorganisms, identifying pathogenic bacteria, and minimizing their impact on human life have long been focal points of research.[1] This issue has become even more critical with the overuse of antibiotics, which has led to the emergence and rapid spread of antibiotic-resistant bacteria, posing a serious threat to global health.[2,3] In response, researchers are actively seeking novel structural strategies to create next-generation antimicrobial materials that combine high efficacy with excellent biosafety. These efforts extend to a diverse array of approaches, including metal nanoparticles,[4,5] antimicrobial peptides,[6,7] antimicrobial polymers,[8–11] and emerging hybrid systems that integrate multiple mechanisms of action.[12–14] In the search for effective antibiotic alternatives, researchers are focused on identifying critical factors that enhance antimicrobial efficacy while minimizing cytotoxicity. Antimicrobial peptides (AMPs) represent a promising class of molecules, typically composed of 10–50 amino acid residues.[7,15] Although this may be an oversimplification, the accepted antibacterial mechanism of AMPs is attributed to their amphiphilic nature, characterized by cationic charges, hydrophobic chains, and hydrophilic groups, which enables them to interact with bacterial membranes, disrupting cell integrity.[16] The positive charges allow AMPs to bind preferentially to the negatively charged components commonly found on bacterial surfaces, such as anionic lipids in the membranes or teichoic acids in Gram-positive bacteria.[17,18] These electrostatic interactions promote selective accumulation on bacterial membranes over mammalian cells. In Gram-negative bacteria, AMPs often first interact with the outer membrane, which contains lipopolysaccharides (LPS), before reaching the inner membrane; in

[a]*Smart and Sustainable Polymeric Products, Engineering and Technology Institute Groningen, University of Groningen, Nijenborgh 4, 9747 AG, The Netherlands. E-mail: p.raffa@rug.nl*
[b]*Biomaterials & Biomedical Technology, University Medical Center Groningen, Antonius Deusinglaan 1, 9713 AV Groningen, The Netherlands*
[c]*Department of Biochemistry, University of Groningen, Nijenborgh 3, 9747 AG Groningen, The Netherlands*
[d]*Department of Industrial Chemistry, University of Bologna, Via Piero Gobetti 85, 40129 Bologna, Italy*

Open Access Article. Published on 22 apríl 2026. Downloaded on 03.06.2026 13:44:47.
This article is licensed under a Creative Commons Attribution 3.0 Unported Licence.

Gram-positive bacteria, although the absence of LPS allows direct access to the cytoplasmic membrane, the thick peptidoglycan layer can also constitute a substantial barrier to AMP penetration.[19,20] Consequently, the efficiency of membrane disruption and pore formation depends strongly on the specific AMPs and bacterial strain, and membrane destabilization remains a common mode of action.[21]

With advancements in controlled polymerization techniques, particularly Reversible Deactivation Radical Polymerization (RDRP), such as Atom Transfer Radical Polymerization (ATRP) and Reversible Addition–Fragmentation chain Transfer (RAFT) polymerization,[22–25] scientists have been able to synthesize numerous amphiphilic antimicrobial polymers that mimic the above-mentioned functional and structural attributes of natural AMPs.[26–33] Recent investigations on synthetic polymers revealed that the molar mass plays a crucial role in determining their biocompatibility. In many reported studies, particularly for linear polymers, an increase in molar mass is associated with heightened cytotoxicity.[34–36] To achieve an optimal amphiphilic balance, hydrophobic and cationic monomers are frequently utilized, with hydrophilic neutral monomers sometimes included.[37–39] Importantly, the addition of these hydrophilic monomers has been demonstrated to significantly enhance biocompatibility. As mentioned above, it is commonly accepted that cationic groups facilitate the adsorption of polymers onto anionic bacterial membranes *via* electrostatic interactions, which has led to extensive research on various cationic moieties to better understand their structural implications for the overall biological activity.[40–43] On the other hand, hydrophobic groups are suggested to disrupt the integrity of bacterial and mammalian membranes, prompting researchers to screen various hydrophobic monomers (including differences in chain length and chemical structure) to improve selectivity.[37,44–46] Overall, both the type and density of cationic groups, as well as the nature of hydrophobic monomers, play crucial roles in determining antimicrobial activity and cytotoxicity.[39,47,48] To address these requirements, cationic amino acid-functionalized monomers have been widely employed in antimicrobial polymer design, owing to their ability to partially reproduce key structural and functional features of AMPs.[49–51] However, two critical limitations remain. First, although amino acid-based monomers have been increasingly used, most synthetic amphiphilic copolymers reproduce only a limited subset of AMPs' compositional features, making it difficult to systematically disentangle the specific contributions of individual amino acid side chains to antimicrobial activity, selectivity, and cytotoxicity. In natural AMP sequences, antimicrobial function arises from a complex interplay of multiple residues and motifs, which together govern membrane affinity, selectivity, and conformational stability.[52] Replicating this level of functional complexity in synthetic polymer systems remains a significant challenge. Second, the hydrophobic components in the majority of reported antimicrobial polymers are still based on fossil-derived monomers, which limits the sustainability of these materials.[37,38,44,47]

With the goal of proposing a more sustainable design for peptide-inspired amphiphilic polymers, in this study, we prepared polymers based on cationic and hydrophobic bio-based monomers. We converted amino acids into the corresponding methacrylates and explored the impact of amino acid side chain variations on the antimicrobial activity of amphiphilic polymers, utilizing amino acids with different side chains (Ala, methyl; Phe, aromatic; Lys, cationic) as the cationic components. Additionally, bio-based tetrahydrogeraniol (THG) was incorporated as the hydrophobic component, *via* modification into the corresponding methacrylate.[53] Beyond its renewable origin, THG provides a moderate and well-balanced hydrophobicity, comparable to that of commonly used short- to medium-chain linear alkyl methacrylates (*e.g.*, C6–C8), while its branched aliphatic structure helps avoid excessive hydrophobicity, which often significantly increases the cytotoxicity of polymers due to excessively long hydrophobic chains.[32,54] Through RAFT controlled polymerization, we successfully synthesized a library of 15 statistical amphiphilic random copolymers with varying ratios of cationic and hydrophobic components. The antimicrobial activity and cytotoxicity of these copolymers were evaluated against Gram-negative *E. coli*, Gram-positive *S. aureus*, and mouse fibroblast cells (*L*929). These findings contribute to a deeper understanding of amphiphilic antimicrobial polymers and may help develop agents with enhanced antimicrobial efficacy and reduced cytotoxicity toward mammalian cells, starting from more sustainable building blocks.

2. Materials and methods

Materials

2,2′-Azobisisobutyronitrile (AIBN), tetrahydrogeraniol (THG), triethylamine (TEA), methacryloyl chloride, Boc-Ala-OH, Boc-Phe-OH, Boc-Lys (Boc)-OH·DCHA, *N*,*N*′-dicyclohexylcarbodiimide (DCC), *N*,*N*-dimethylpyridin-4-amine (DMAP), trifluoroacetic acid (TFA), 2-hydroxyethyl methacrylate (HEMA), 4-cyano-4-[(dodecylsulfanylthiocarbonyl)sulfanyl]pentanoic acid, calcein, phosphatidylcholine (PC), sodium bicarbonate ($NaHCO_3$), anhydrous sodium sulfate (Na_2SO_4), sodium chloride (NaCl), potassium bisulfate ($KHSO_4$), hydrochloric acid (HCl), dimethylformamide (DMF), dichloromethane (DCM), and dimethyl sulfoxide (DMSO) were purchased from Sigma-Aldrich. Phosphate buffered saline (PBS) and Roswell Park Memorial Institute (RPMI) 1640 medium were purchased from Gibco. The Cell Proliferation Kit XTT was purchased from PanReac AppliChem, and a LIVE/DEAD BacLight Bacterial Viability Kit was bought from Thermo Fisher Scientific (catalog number L7012). The bacteria and cells were obtained from ATCC: *E. coli* (ATCC 25922); *S. aureus* (ATCC 6538); and mouse fibroblast cells (*L*929 (ATCC CCL-1)).

Synthesis of monomers

Tetrahydrogeranyl methacrylate, THGA.[53] In a three-neck 500 mL round-bottomed flask equipped with a rubber seal, a

 This journal is © The Royal Society of Chemistry 2026

Open Access Article. Published on 22 aprel 2026. Downloaded on 03.06.2026 13:44:47.
This article is licensed under a Creative Commons Attribution 3.0 Unported Licence.

dropping funnel and a magnetic stirrer, THG (9.50 g, 0.06 mol), TEA (6.07 g, 0.06 mol) and DCM (180 mL) were added. The mixture was placed in an ice bath and cooled with stirring for 2 hours. Subsequently, methacryloyl chloride (8.15 g, 0.09 mol) was added dropwise through a dropping funnel. After the addition was complete, the mixture was stirred in the ice bath for 1 hour and stirred at ambient temperature for 24 hours. Then, the mixture was suction filtered and the mixture was washed several times with brine (150 mL) and deionized water (150 mL). The organic phase solvent was removed by rotary evaporation to obtain a light yellow transparent viscous liquid (12.48 g, 92% yield).

^{1}H NMR (400 MHz, $CDCl_3$) δ 6.09 (dt, J = 2.0, 1.0 Hz, 1H), 5.54 (p, J = 1.6 Hz, 1H), 4.25–4.11 (m, 2H), 1.94 (dd, J = 1.6, 1.0 Hz, 3H), 1.70–1.66 (m, 1H), 1.55–1.48 (m, 3H), 1.34–1.10 (m, 6H), 0.89 (dd, J = 20.5, 6.6 Hz, 9H).

^{13}C NMR (101 MHz, $CDCl_3$) δ 167.56, 136.56, 125.11, 63.28, 39.17, 37.11, 35.47, 29.92, 27.93, 24.60, 22.66, 22.58, 19.57, 18.31.

Boc-amino acid-HEMA.[55] In brief, for the synthesis of Boc-Ala-HEMA, Boc-Ala-OH (26.43 mmol, 5.0 g) was dissolved in 100 mL of anhydrous DCM in a 250 mL two-neck round-bottom flask equipped with a magnetic stir bar, and the solution was purged with anhydrous N_2 for 20 minutes. Under a N_2 atmosphere, DCC (29.07 mmol, 6.00 g) was dissolved in 30 mL of DCM and added dropwise with vigorous stirring. After the addition, DMAP (1.32 mmol, 0.16 g) was added. The reaction flask was then transferred to an ice-water bath, and HEMA (26.43 mmol, 3.44 g) was added dropwise. The mixture was stirred in the ice bath for 30 minutes and then stirred at room temperature for 24 hours. The reaction mixture was filtered, and the filtrate was washed sequentially with 0.1 N HCl (4 × 200 mL), saturated $NaHCO_3$ (4 × 200 mL), and brine (2 × 100 mL). The filtrate was dried over anhydrous Na_2SO_4. The solvent was removed by rotary evaporation to yield a colorless viscous liquid, identified as Boc-Ala-HEMA (91% yield).

The synthesis methods for Boc-Phe-HEMA (93% yield) and Boc-Lys(Boc)-HEMA (95% yield) are identical. Notably, for the purchased Boc-Lys(Boc)-OH·DCHA salt, a pre-treatment was required. The precursor was first dissolved in DCM, and the solution was then extracted three times with a cold $KHSO_4$ aqueous solution. The organic layer was dried over Na_2SO_4 and filtered, and the solvent was removed under reduced pressure to obtain the free Boc-Lys(Boc)-OH acid.

Boc-Ala-HEMA. ^{1}H NMR (400 MHz, $CDCl_3$) δ 6.13–6.11 (m, 1H), 5.59 (p, J = 1.6 Hz, 1H), 4.46–4.40 (m, 1H), 4.39–4.31 (m, 4H), 1.94 (dd, J = 1.6, 1.0 Hz, 3H), 1.44 (s, 12H).

^{13}C NMR (101 MHz, $CDCl_3$) δ 173.15, 167.03, 153.62, 135.81, 126.16, 125.99, 80.23, 62.82, 62.16, 50.14, 28.32, 28.28, 28.26, 18.59, 18.22.

Boc-Phe-HEMA. ^{1}H NMR (400 MHz, DMSO) δ 7.37–7.13 (m, 5H), 6.02 (s, 1H), 5.71–5.63 (m, 1H), 4.38–4.03 (m, 4H), 2.95 (dd, J = 13.8, 5.1 Hz, 1H), 2.83 (dd, J = 13.8, 9.9 Hz, 1H), 1.85 (t, J = 1.3 Hz, 2H), 1.34–1.04 (m, 9H).

^{13}C NMR (101 MHz, $CDCl_3$) δ 171.69, 167.03, 155.04, 135.87, 135.80, 129.26, 128.55, 127.07, 126.23, 79.95, 62.94, 62.17, 54.35, 38.27, 28.26, 18.25.

Boc-Lys(Boc)-OH free acid. ^{1}H NMR (400 MHz, $CDCl_3$) δ 5.22 (s, 1H), 4.63 (s, 1H), 4.29 (s, 1H), 3.12 (d, J = 6.5 Hz, 2H), 1.79 (d, J = 49.5 Hz, 2H), 1.44 (d, J = 3.5 Hz, 22H).

^{13}C NMR (101 MHz, $CDCl_3$) δ 176.22, 156.31, 155.81, 80.06, 79.35, 53.25, 40.06, 31.97, 29.51, 28.40, 28.32, 22.37.

Boc-Lys(Boc)-HEMA. ^{1}H NMR (400 MHz, $CDCl_3$) δ 6.12 (dd, J = 2.2, 1.1 Hz, 1H), 5.60 (p, J = 1.6 Hz, 1H), 4.47–4.23 (m, 5H), 3.09 (d, J = 7.4 Hz, 2H), 1.94 (dd, J = 1.6, 1.0 Hz, 3H), 1.68 (d, J = 8.2 Hz, 2H), 1.43 (s, 23H).

^{13}C NMR (101 MHz, $CDCl_3$) δ 172.57, 167.00, 156.03, 135.81, 126.19, 79.89, 62.83, 62.17, 53.24, 40.01, 32.26, 29.56, 28.40, 28.29, 22.42, 18.23.

Synthesis of Boc-protected random copolymers

Typically, Boc-Ala-HEMA and THGA (in varying ratios, totaling 10 mmol) were dissolved in 5 mL of 1,4-dioxane, followed by the addition of the RAFT chain transfer agent 4-cyano-4-[(dodecylsulfanylthiocarbonyl)sulfanyl]pentanoic acid (5% of the total monomer amount, 0.5 mmol) and the initiator AIBN (8 mg, 0.05 mmol). The mixture was purged with nitrogen for 15 minutes and then stirred at 70 °C. After 18 hours, the reaction was terminated by cooling the vial in an ice bath. The copolymer was isolated by evaporating the dioxane under reduced pressure, dissolving the residue in dichloromethane, and precipitating twice in an excess of *n*-hexane (or in a 9 : 1 ethanol–water mixture for polymers with high THGA content) to remove unreacted impurities. The sample was then dried overnight in a vacuum oven at 40 °C, yielding a light-yellow solid copolymer.

Deprotection of copolymers

The Boc-protected random copolymer (1 g) was combined with TFA (1 mL).[55] After stirring for 30 minutes, TFA was removed by purging with nitrogen. The remaining residue was dissolved in water, and impurities were removed using a 3500 Da dialysis bag for 3 days. The copolymer solution in the dialysis bag was then lyophilized using a freeze dryer to obtain a light, fluffy, white fibrous copolymer. NMR analysis was used to determine the removal of Boc protective groups.

^{1}H NMR spectroscopy

NMR spectroscopy was used to analyze all the Boc-protected and de-protected copolymers to analyze polymer composition and conversion. Analysis was performed to determine the mole percent of THGA (MP_{THGA}), degree of polymerization (DP), and number-average molecular weight (M_n). All experiments were performed using an Agilent 400 MHz WB NMR spectrometer. All experiments were run with a gas flow across the probes at 535 L h^{-1} with sample spinning and at a temperature of 25 °C.

Size exclusion chromatography (SEC)

The copolymers were also characterized by SEC analysis to measure the M_n, weight-average molecular weight (M_w) and dispersity ($Đ$) using DMF (containing 0.01 M LiBr) as an eluent

Open Access Article. Published on 22 apríl 2026. Downloaded on 03.06.2026 13:44:47.
This article is licensed under a Creative Commons Attribution 3.0 Unported Licence.

in a Viscotek GPCmax instrument equipped with a model 302 TDA detector based on the refractive index and intrinsic viscosity and two columns (Agilent Technologies – PolarGel-L and M, 8 μm, 30 cm) at a flow rate of 1.0 mL min^{-1} and a temperature of 50 °C. A universal calibration curve was prepared using narrow dispersion poly(methyl methacrylate) (PMMA) standards (Polymer Laboratories). Polymer solutions of 2 mg mL^{-1} in DMF were prepared in the eluent and filtered through 0.45 μm filters prior to injection.

Dynamic light scattering (DLS) and zeta potential (ζ) measurements

For those polymers that could self-assemble into aggregates in aqueous solution, a Malvern Zetasizer Nano ZS (Malvern Instruments, Worcestershire, UK) instrument equipped with a HeNe laser was used with a wavelength of λ = 633 nm and a scattering angle of 173°. The data were computed using cumulant fit analysis and the hydrodynamic diameter size (D_h) was calculated using the Stokes–Einstein equation with the software. The ζ value was determined from the electrophoretic mobility of the particles by applying the Smoluchowski equation. All polymers were measured at a concentration of 1 mg mL^{-1} in PBS (the solutions were filtered using a 0.22 μm pore size filter). Final data for the size and ζ of the particles were calculated as the average of three consecutive measurements of the same sample.

Transmission electron microscopy (TEM)

The morphology of the nanoscale aggregates was analyzed *via* TEM using a Philips CM120 operating at 120 keV. Images were recorded using a Gatan model UltraScan 4000SP CCD camera under low-dose conditions. All polymers were measured at concentrations of 0.1–0.5 mg mL^{-1} in PBS (using a 0.22 μm pore size filter) and 10 μl of the polymer solution was placed on a carbon-coated copper grid (Quantifoil 3.5/1, Quantifoil Micro Tools, Jena, Germany). Then, samples were negatively stained with 2% uranyl acetate, and the excess solution was blotted off and dried at room temperature for a few minutes before measurement.

Zone of inhibition experiment

Briefly, a single colony of microorganisms was picked from the agar plate, inoculated into Mueller–Hinton broth (MHB; 50 mL) and cultured at 37 °C for 12 h. Fresh colonies were then collected by centrifugation (6500 rpm, 5 min) and washed three times with PBS to remove the remaining culture medium. Then, the microbial solution was diluted to 1.0×10^8 CFU mL^{-1} with PBS, 100 μL were taken and spread evenly on the agar plate, 10 μL of random copolymers (10 mg mL^{-1} in PBS or 10% DMSO in PBS was used as a solvent for insoluble samples) with the same content were added to different positions of the plate, and then the plate was incubated at 37 °C for 18 hours; the antibacterial activity was evaluated by measuring the inhibition zone.

The minimum inhibitory concentration (MIC) and minimum bactericidal concentration (MBC) tests

Random copolymers were initially dissolved in PBS to achieve a stock concentration of 20 mg mL^{-1}. For polymers that were insoluble in PBS, PBS containing up to 10% DMSO was used to ensure complete dissolution. Serial 2-fold dilutions of polymers were prepared from the stock solutions in PBS and transferred to the 96-well sterile round-bottom polypropylene plate for final concentrations of 7.8–2000 μg mL^{-1} (10 μL per well). PBS and 10% DMSO in PBS were used as solvent controls. Bacteria were grown overnight (~18 hours) in MHB at 37 °C, and fresh colonies were then collected by centrifugation (6500 rpm, 5 min) and washed three times with PBS to remove the remaining culture medium. Then, the microbial solution was diluted to 4×10^5 CFU mL^{-1} (the counting and the culture dilution were performed using Bürker-Türk counting chambers) with MHB. The bacterial suspension (90 μL per well) was transferred to a 96-well sterile round-bottom polypropylene plate. Then, the polymer solution was diluted to a final concentration of 7.8–2000 μg mL^{-1} (10 μL per well). The plate was sealed with parafilm and incubated for 18 hours at 37 °C without shaking. The MIC was defined as the lowest concentration of polymers to completely inhibit bacterial growth, as indicated by the lack of turbidity.

After the MIC test, the MBC test was carried out directly. For each sample, from the concentration where no bacterial growth was observed to the concentration where turbid growth occurred, 10 μL of each test concentration was spotted on an agar plate and incubated at 37 °C for 24 hours. The lowest concentration where no bacteria survived was defined as the MBC.

Cytotoxicity assay

The Cell Proliferation Kit XTT[56,57] (PanReac AppliChem) was used to assess *in vitro* cytotoxicity using mouse fibroblast cells (*L*929). *L*929 cells were grown in complete medium (RPMI 1640, Gibco), until reaching subconfluency at 37 °C and 5% CO_2 in a cell culture incubator (Eppendorf CellXpert C170i). A 96-well cell culture plate was used to seed the cells (10^4 cells per well). After 24 h, the growth medium was replaced with RPMI 1640 medium consisting of different polymer concentrations, and two-fold serial dilutions were performed starting from 5000 μg mL^{-1} with/without the polymer (with PBS-treated wells as the negative control). Cell viability was normalized to the negative control and defined as 100%. After a further 24 hours of incubation in the incubator (the polymer continued to expose cells), 50 μl of reaction solution (from the kit) was added to each well and the plate was placed in the incubator for 2 hours. The absorbance of the samples relative to the background control was measured at 475 nm using a microplate reader (BioTek Synergy H1) at a wavelength of 475 nm. In order to measure reference absorbance (to measure non-specific readings), a wavelength of 660 nm was used and subtracted from the 475 nm measurement.

The following formula was used to calculate the percentage of cell viability:

$$\text{Cell viability (\%)} = \frac{[\text{OD}_{660}(\text{test sample}) - \text{OD}_{475}(\text{test sample})]}{[\text{OD}_{660}(\text{negative control}) - \text{OD}_{475}(\text{negative control})]} \times 100\%$$

This journal is © The Royal Society of Chemistry 2026

Open Access Article. Published on 22 aprel 2026. Downloaded on 03.06.2026 13:44:47.
This article is licensed under a Creative Commons Attribution 3.0 Unported Licence.

where OD_{475} is the absorbance at 475 nm; OD_{660} is the absorbance at 660 nm; (test sample) corresponds to the average of the observed results of 3 wells, and (negative control) refers to the average of 9 control wells with medium.

Live/dead membrane integrity assay

Bacterial cell membrane integrity was studied using the LIVE/DEAD BacLight Bacterial Viability Kit[58,59] (bought from Thermo Fisher Scientific (catalog number L7012)). The kit utilized mixtures of the SYTO9 green fluorescent nucleic acid stain and the red-fluorescent nucleic acid stain, propidium iodide. Bacterial cells with a compromised membrane that were dead or dying would stain red with propidium iodide, whereas cells with an intact membrane would stain green with SYTO9. The bacterial suspension of 10^8 cells mL^{-1} in PBS was incubated in the absence (as control) or presence of different concentrations (MIC and 4× MIC) of polymer for 4 h at 37 °C. After that the bacteria were harvested by centrifugation and washed with PBS 3 times. Then, the bacteria were resuspended in a 0.9% salt solution to reach a final density of 1×10^6 cells mL^{-1}. 10 μL of the bacterial suspension was added to 3 μL of the dye mixture (SYTO9 with propidium iodide 1 : 1). Sample solutions were mixed well and incubated in the dark at room temperature for 15 min. Then, they were examined by confocal laser scanning microscopy (CLSM, DM4000B, Leica).

Scanning electron microscopy (SEM)

Bacteria were collected by centrifugation, and washed cells (after washing with PBS three times) were adhered to slides and fixed with 2% glutaraldehyde for 10 min at 4 °C. They were then washed with 0.1 M cacodylate buffer, incubated with 1% OsO_4 in 0.1 M cacodylate buffer for 1 h at room temperature, washed with water, and then dehydrated using a series of graded ethanol solutions (30, 50, 70%) for 15 min each at room temperature, and finally, they were dehydrated three times with 100% ethanol for 30 min each and then dried. The dehydrated samples were gold-coated for 20 s and imaged under high vacuum using a Supra 55 Scanning Electron Microscope (Zeiss).

Lipid vesicle preparation

A lipid mixture composed of *E. coli* polar lipids and egg PC in a 3 : 1 molar ratio was prepared for vesicle formation. *E. coli* polar lipids were obtained from a commercial total lipid extract (Avanti Polar Lipids) by acetone precipitation followed by diethyl ether extraction, as described in ref. 60. Both *E. coli* lipids and egg PC were dissolved in chloroform and mixed, and the solvent was evaporated using a rotary evaporator (Büchi Labortechnik AG). The resulting lipid film was washed with diethyl ether, then hydrated in 50 mM potassium phosphate (pH 7.0) to a final concentration of 20 mg mL^{-1}. The lipid suspension was sonicated using a tip sonicator (70% amplitude, 15 s on/45 s off, 16 cycles) while kept on ice, and then subjected to three freeze–thaw cycles (liquid nitrogen and room-temperature water bath). The prepared large-unilamellar vesicles (LUVs) were aliquoted and stocked in liquid nitrogen to prevent oxidation.

Liposome preparation for a calcein leakage experiment

A 100 mM calcein stock solution was prepared in 50 mM potassium phosphate buffer (KPi) and adjusted to pH 7.0 using 2 M NaOH (Sigma-Aldrich). Liposomes were resuspended in a solution containing 70 mM calcein and 20 mM KPi (pH 7.0) to a final lipid concentration of 5 mg mL^{-1}. Calcein, at a self-quenching concentration, was encapsulated into the vesicles by subjecting the suspension to three freeze–thaw cycles at 30 °C. Following this, the vesicle suspension was extruded 13 times through a 200 nm polycarbonate membrane (Whatman, GE Healthcare) to obtain large-unilamellar vesicles (LUVs). Unencapsulated calcein was removed *via* size-exclusion chromatography using a 22 cm Sephadex G-75 column (Sigma-Aldrich) pre-equilibrated with an iso-osmotic buffer composed of 50 mM KPi (pH 7.0) plus 50 mM sucrose. Fractions (1 mL each) containing calcein-loaded liposomes were identified under ultraviolet illumination and pooled. The final vesicle suspension was diluted to a total volume of 12 mL in the same buffer (KPi 50 mM, pH 7.0, sucrose 50 mM).

Calcein leakage experiment

The ability of the polymer to induce membrane lysis or pore formation was assessed using a calcein leakage assay. Calcein-loaded vesicles were incubated with increasing concentrations of the polymer (0–1000 μg mL^{-1}), and the release of calcein was monitored as an increase in fluorescence intensity. Measurements were performed using a Spark Multimode Plate Reader (TECAN) at 25 °C, with an excitation wavelength of 495 nm and emission recorded at 517 nm. Fluorescence was measured every minute for a total of 30 minutes, until a fluorescence plateau was reached. Afterward, Triton X-100 (50% w/w) was added to fully disrupt the vesicles and determine the maximum fluorescence signal, $F(\max)$.

The percentage of calcein leakage was calculated according to the following equation:

$$\text{Leakage}\,(\%) = \frac{F(t) - F(0)}{F(\max) - F(0)} \times 100$$

where $F(0)$ is the fluorescence at time 0 (prior to polymer addition), $F(t)$ is the fluorescence at a given time point after polymer addition, and $F(\max)$ is the fluorescence after complete dissolution of vesicles with Triton X-100.

Each measurement was performed in triplicate.

3. Results and discussion

Polymer synthesis and characterization

In this study, the synthetic route shown in Fig. 1 was used to functionalize the bio-based starting material by introducing carbon–carbon double bonds into the Boc-protected amino acid moieties (Ala, methyl; Phe, aromatic; Lys, cationic) and THG. The ^1H and ^{13}C NMR characterization studies confirmed

Open Access Article. Published on 22 apríl 2026. Downloaded on 03.06.2026 13:44:47.
This article is licensed under a Creative Commons Attribution 3.0 Unported Licence.

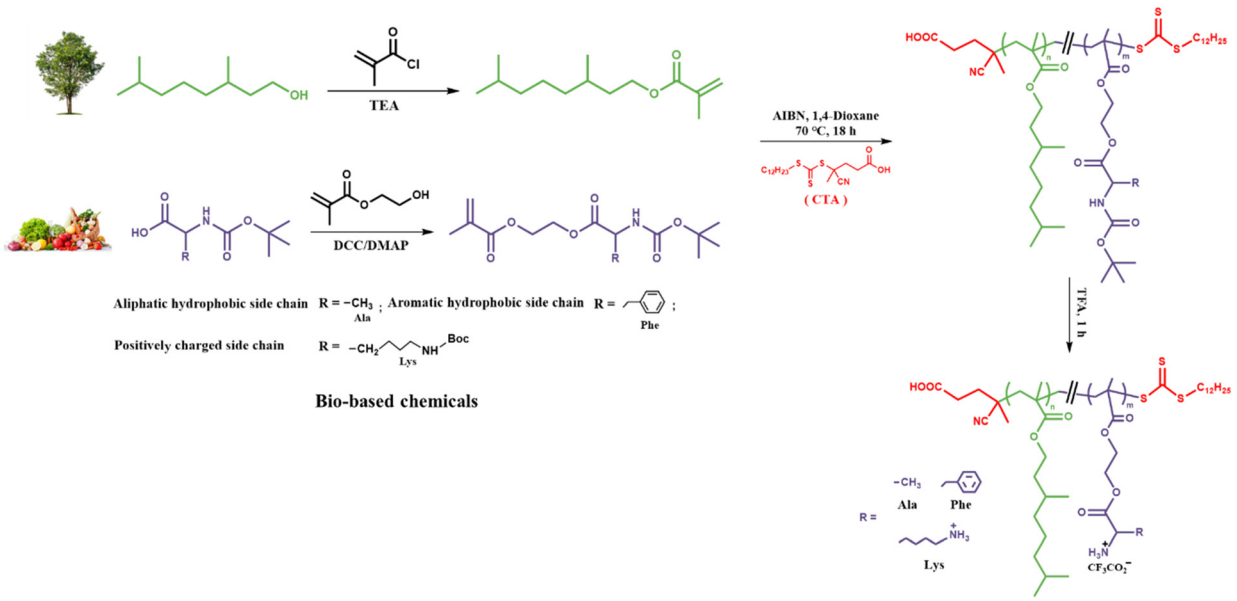

Fig. 1 Schematic diagram of the synthesis of bio-based monomers and amphiphilic random copolymers by RAFT polymerization.

that the monomer was successfully synthesized (Fig. S1–S10). Then, a library of amphiphilic copolymers was successfully synthesized using Reversible Addition–Fragmentation chain-Transfer (RAFT) polymerization (Fig. 1).[61] Specifically, to closely approximate the molar mass of antimicrobial peptides (several kDa) and avoid increased cytotoxicity associated with higher molar mass, all polymers were prepared with a target DP of 20, with the Chain Transfer Agent (CTA) constituting 5% of the total molar amount of monomers. The polymers include three components: (1) cationic groups, represented by three amino acids with different side chains – Ala (methyl side chain), Phe (aromatic phenyl ring), or Lys (positively charged amino side chain); (2) hydrophobic monomer, derived from bio-based THG and modified with a double bond to form THGA; and (3) end-groups from the CTA, specifically CDPA, which contains a long aliphatic chain.

By adjusting the ratio of cationic monomers to hydrophobic monomers, a series of amphiphilic random copolymers with varying molar ratios between the two components were synthesized to study their structure–activity relationships. Based on the cationic component, the polymers were classified into three major families: alanine group (A family), phenylalanine group (P family), and lysine group (L family). The hydrophobic monomer was THGA for all polymers. The polymers were named P(*x*-r-T)*y*, where *x* indicates the type of amino acid (A, P or L), and *y* is a number from 1 to 9, corresponding to the relative amount of cationic monomer (from 10 to 90%). For example, in P(A-r-T)1, A corresponds to the cationic monomer with Ala, r stands for random, T corresponds to the hydrophobic monomer THGA, and number 1 indicates 10 mol% of the cationic monomer (and 90 mol% of the hydrophobic one).

All the copolymers (with and without Boc deprotection) prepared *via* RAFT polymerizations were analyzed by ^{1}H NMR and SEC to determine the monomer conversion (% conv.), molecular weights (M_n and M_w), copolymer composition (MP_{THGA} (%)), and $Đ$ (Table 1). The ^{1}H NMR analysis results of the reaction solutions before and after the reaction were compared, and the monomer conversion was calculated by comparing the vinyl proton signals at 5.5 and 6.3 ppm with the solvent peak (Fig. S11), indicating that the monomer conversion of all prepared polymers exceeded 80%, with only the reaction monomer conversion of P(A-r-T)3 being 75.2%. The M_n value was estimated by SEC and ^{1}H NMR with good agreement between theoretical M_n and experimental values. The average DP was calculated by comparing the integral peak areas of the side chain terminal groups and main chain end groups (Fig. S13, S15 and S17). The MP_{THGA} value was determined by comparing the signals generated by the two different side chains in the ^{1}H NMR spectra. For each copolymer series, the fraction of hydrophobic repeating units (THGA) in the copolymer, MP_T, ranged from 10% to 90%, consistent with the monomer feed ratios. The SEC results (Fig. S21) showed that the molecular weights (3 to 4 kDa) and $Đ$ values (1.2 to 1.4) indicate that the polymerization reaction was well controlled. After deprotection of the Boc group with TFA, the signal at about 1.4 ppm (attributed to the protons of the *tert*-butyl group) disappeared in the ^{1}H NMR spectrum of the polymer, confirming successful removal of the Boc protecting group.

The water solubility of the random copolymers also correlates with the increasing content of cationic components. In the Ala series random copolymers, which have methyl side chains, the polymers become water-soluble when the cationic content reaches approximately 70%. In contrast, the Phe series polymers, bearing more hydrophobic phenyl side chains, remain insoluble regardless of cationic content. For the Lys series, which contains 2 cationic side chains per monomer,

 This journal is © The Royal Society of Chemistry 2026

Open Access Article. Published on 22 april 2026. Downloaded on 03.06.2026 13:44:47.
This article is licensed under a Creative Commons Attribution 3.0 Unported Licence.

Table 1 Polymer characterization by ^{1}H NMR, SEC, DLS and zeta potential analyses

Random copolymers	Theoretical composition (%)	% conv.[a]	Boc-protected						Deprotected								
			MP_{THGA}[b] (%)	M_n[c]	DP[d]	M_n[e]	M_w[e]	D[e]	MP_{THGA}[b] (%)	M_n[c]	DP[d]	M_n[e]	M_w[e]	D[e]	H_2O sol	D_h[f] (nm)	ζ[g] (mV)
P(A-r-T)1	10(Ala) : 90(THGA)	90.2	85	3750	14	3400	4080	1.20	93	3570	14	2800	3900	1.41	✗	nd	nd
P(A-r-T)3	30(Ala) : 70(THGA)	75.2	72	3660	13	3900	5000	1.28	75	3320	13	3300	4400	1.35	✗	nd	nd
P(A-r-T)5	50(Ala) : 50(THGA)	90.9	49	4180	14	5000	6200	1.25	50	3350	14	4000	5800	1.45	✗	nd	nd
P(A-r-T)7	70(Ala) : 30(THGA)	83.9	30	5290	17	5000	6200	1.25	34	3960	17	3600	5000	1.38	✓	25.6	nd
P(A-r-T)9	90(Ala) : 10(THGA)	89.6	13	5709	18	5000	6200	1.23	26	3420	16	3500	4900	1.41	✓	53.9	+8.2
P(P-r-T)1	10(Phe) : 90(THGA)	87.4	91	3620	15	3500	4400	1.25	93	nd	nd	3000	4000	1.35	✗	nd	nd
P(P-r-T)3	30(Phe) : 70(THGA)	91.8	66	4180	14	4500	5500	1.22	76	4140	15	3400	4600	1.37	✗	nd	nd
P(P-r-T)5	50(Phe) : 50(THGA)	92.7	47	5190	15	4800	6100	1.27	54	4350	15	3700	4900	1.31	✗	nd	nd
P(P-r-T)7	70(Phe) : 30(THGA)	93.5	27	5170	14	5200	6400	1.25	34	nd	nd	3700	5000	1.35	✗	nd	nd
P(P-r-T)9	90(Phe) : 10(THGA)	94.3	11	5520	14	5500	6600	1.18	11	nd	nd	3400	4400	1.28	✗	nd	nd
P(L-r-T)1	10(Lys) : 90(THGA)	91.6	84	5480	19	5100	5600	1.10	91	4980	20	nd	nd	nd	✗	nd	nd
P(L-r-T)3	30(Lys) : 70(THGA)	94.2	71	6820	21	5200	5800	1.12	81	4560	18	nd	nd	nd	✗	nd	nd
P(L-r-T)5	50(Lys) : 50(THGA)	96.8	51	5760	16	5900	7100	1.09	53	nd	nd	nd	nd	nd	✓	48.1	+21.6
P(L-r-T)7	70(Lys) : 30(THGA)	93.5	34	7070	18	6600	7200	1.08	29	nd	nd	nd	nd	nd	✓	59.0	+18.5
P(L-r-T)9	90(Lys) : 10(THGA)	93.3	19	nd	nd	6300	7300	1.15	13	nd	nd	nd	nd	nd	✓	64.6	+13.4

[a] % conv. (% monomer conversion during polymerization) determined by ^{1}H NMR peak integration analysis. [b] MP_{THGA} (mole percentage of hydrophobic side chains) determined by ^{1}H NMR peak integration analysis. [c] M_n (number average molecular weight) determined by ^{1}H NMR peak integration analysis. [d] DP (degree of polymerization) values determined by ^{1}H NMR peak integration analysis. [e] M_n, M_w, and dispersity (D) determined by SEC analysis in DMF against PMMA standards. [f] D_h (hydrodynamic number average diameter size) determined using a Malvern Zetasizer Nano ZS at a concentration of 0.1 mg mL^{-1} in PBS. [g] ζ (zeta potential) determined using a Malvern Zetasizer Nano ZS at a concentration of 0.1 mg mL^{-1} in PBS. nd – cannot be determined, indicating one of the following: (i) the NMR peak assignment is unclear because the polymer aggregates in the deuterated reagent after deprotection; (ii) the insolubility of the polymer in THF prevents SEC measurement; or (iii) the insolubility of the polymer in PBS prevents DLS measurement.

water solubility is achieved when the cationic component reaches around 50%. Subsequently, the amphiphilic polymers that could be dissolved in water were also characterized in aqueous media. All characterized polymers have positive ζ (8–21 mV) due to the cationic charge of the amino groups (Table 1). These low ζ values may be due to the difficulty of random copolymers in forming uniform and stable micelles and the partial shielding of cationic charges by polymer intra- and inter-chain interactions. It can be pointed out here that lower stability of the aggregates should be beneficial for the antimicrobial activity, as the polymers most likely interact with the membrane as single chains. Random copolymers with Ala and Lys as cationic components all showed a clear trend of increasing self-assembled aggregate size with the increase of cationic components (Ala or Lys) (Fig. 2a and b), suggesting that the more cationic polymers have larger aggregation numbers. Despite the lower ζ, TEM images confirmed the formation of sufficiently stable nanoscale aggregates (Fig. 2c). The aggregates seem irregular in shape and have sizes below 10 nm. This is obviously smaller than the hydrodynamic sizes obtained by DLS. This is because TEM is performed on dry samples under vacuum, and dehydration can also cause the nanoscale aggregates to shrink or disintegrate. Also, DLS measures the hydrodynamic diameter of the hydrated shell, so the measured diameter is larger than that observed by TEM.[62] Furthermore, because the TEM-observed aggregates are only a few nanometers in size, this approaches the resolution limit of TEM, making it difficult to reliably compare aggregate sizes between samples.

Antimicrobial activity

The antimicrobial activity of the polymers was evaluated by determining the MIC (the lowest concentration of the polymer that inhibited visible bacterial growth) and the MBC (the lowest concentration of the polymer at which the bacteria could not survive): the Gram-negative bacterium *E. coli* (strain ATCC 25922) and the Gram-positive bacterium *S. aureus* (strain ATCC 6538) (Table 2) were tested. Due to the limited water solubility of the polymers, DMSO was used as a cosolvent.

As previously mentioned, these kinds of antimicrobial polymers are believed to kill bacteria mainly *via* membrane disruption.[63,64] These amphiphilic polymers contain cationic and hydrophobic groups, each serving a distinct function. The cationic groups attract anionic components on the surface of bacterial cell membranes through electrostatic interactions, promoting the adsorption of the polymer onto the membrane while compromising membrane integrity and disrupting the transport of compounds across it.[65–67] Simultaneously, the interaction between the cationic groups and the cell membrane induces the polymer to adopt an overall amphiphilic conformation, allowing the hydrophobic groups to insert into the membrane, leading to membrane disruption and cell death.[68,69]

For the Gram-negative bacteria *E. coli*, among the random copolymers composed of Ala and Phe, only the samples with the highest cationic content (up to 90%) showed measurable

Open Access Article. Published on 22 april 2026. Downloaded on 03.06.2026 13:44:47.
This article is licensed under a Creative Commons Attribution 3.0 Unported Licence.

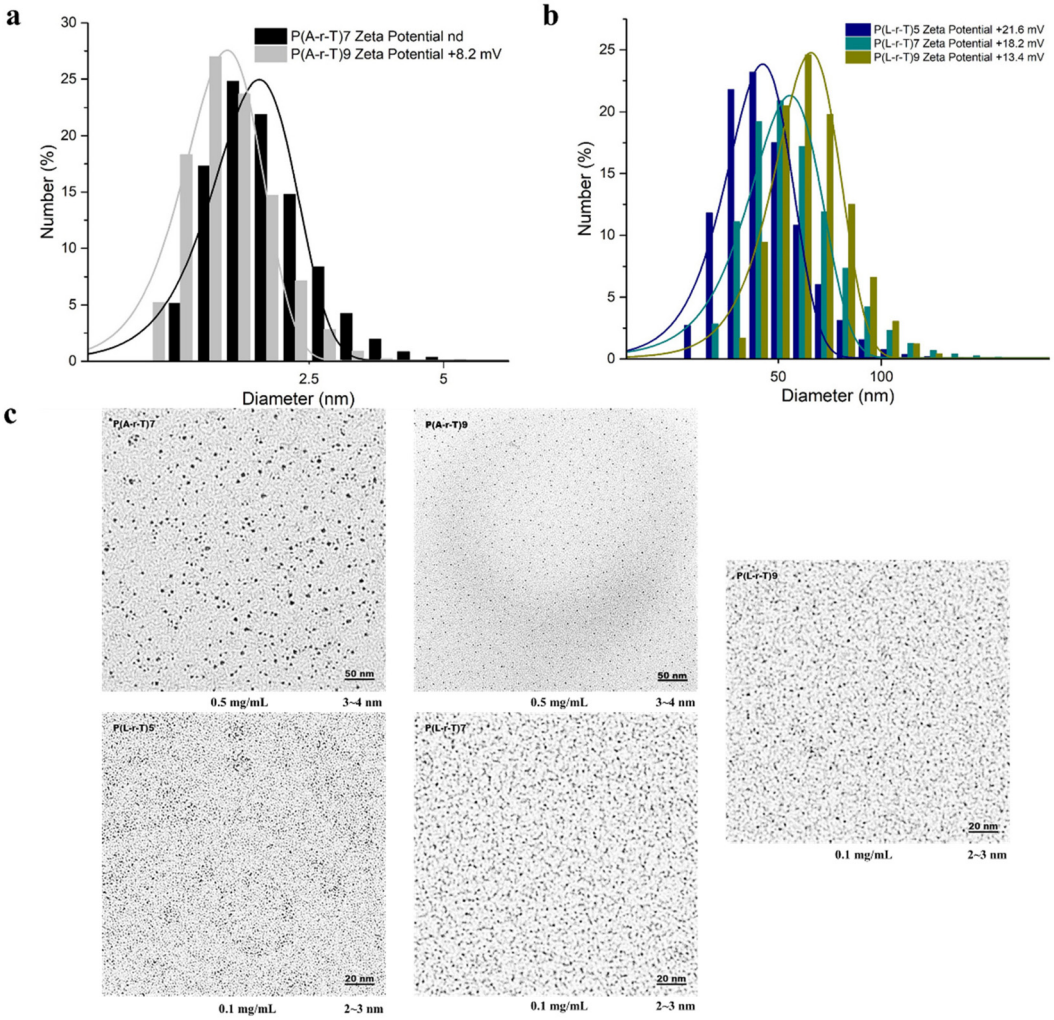

Fig. 2 (a) DLS number size distributions of Ala series water-soluble copolymers in PBS solution (0.1 mg mL^{-1}). (b) DLS number size distributions of Lys series water-soluble copolymers in PBS solution (0.1 mg mL^{-1}). (c) TEM images of nanoscale aggregates formed by water-soluble antibacterial copolymers in PBS.

Table 2 Antimicrobial activity (MIC and MBC) of random copolymers with varying cationic monomers and monomer feed ratios against *E. coli* (ATCC 25922) and *S. aureus* (ATCC 6538)

	MIC (μg mL^{-1})		MBC (μg mL^{-1})	
Random copolymers	*E. coli* (ATCC 25922)	*S. aureus* (ATCC 6538)	*E. coli* (ATCC 25922)	*S. aureus* (ATCC 6538)
P(A-r-T)1	>5000	500	>10 000	>2000
P(A-r-T)3	>5000	2000	>10 000	>2000
P(A-r-T)5	>5000	2000	>10 000	>2000
P(A-r-T)7	>5000	500	>5000	1000
P(A-r-T)9	2500	>2000	5000	>2000
P(P-r-T)1	>5000	250	>10 000	>2000
P(P-r-T)3	>5000	2000	>10 000	>2000
P(P-r-T)5	>5000	2000	>10 000	>2000
P(P-r-T)7	>5000	2000	>10 000	>2000
P(P-r-T)9	5000	1000	5000	>2000
P(L-r-T)1	>5000	500	10 000	>2000
P(L-r-T)3	>5000	1000	10 000	>2000
P(L-r-T)5	1000	1000	5000	>2000
P(L-r-T)7	250	2000	2000	>2000
P(L-r-T)9	125	500	2000	500

antibacterial activity, which may be strictly correlated with their water solubility; however, their MICs were very high (2500 and 5000 μg mL^{-1}, respectively), indicating that these polymers are unlikely to be suitable for prospective *in vivo* applications. In contrast, for the Lys-based copolymers, increasing the cationic monomer content gradually enhanced the polymer antibacterial activity, with the MICs decreasing from 1000 μg mL^{-1} for P(L-r-T)5 to 125 μg mL^{-1} for P(L-r-T)9. For the Gram-positive bacteria *S. aureus*, the balance between the cationic part and the hydrophobic chain with Ala, Phe and Lys had a more obvious effect on the MIC. As the content of the hydrophobic chain decreased, the antibacterial activity first weakened and then increased, with the exception of P(A-r-T)9. Among them, the most hydrophobic one, P(P-r-T)1, showed the lowest MIC (250 μg mL^{-1}), followed by P(A-r-T)1, P(A-r-T)7, P(L-r-T)1, and P(L-r-T)9, with MICs of 500 μg mL^{-1}. The MBCs of the random copolymers tested were all higher than the MIC. Only P(L-r-T)9 with the strongest antibacterial activity had the

 This journal is © The Royal Society of Chemistry 2026

Open Access Article. Published on 22 apríl 2026. Downloaded on 03.06.2026 13:44:47.
This article is licensed under a Creative Commons Attribution 3.0 Unported Licence.

same MBC and MIC against *S. aureus*, which was 500 μg mL^{-1}. As reported in the previous section, the studied polymers are either insoluble in water, or they form relatively stable aggregates. The low value of ζ suggests that the aggregates are labile enough to allow the polymers to interact with the bacterial membranes as single chains.

The results of the zone of inhibition experiments are shown in Fig. S22 and S23. For *E. coli*, it can be clearly seen that there was no growth in the areas where P(L-r-T)7 and P(L-r-T)9 were applied, while *E. coli* grew in the areas where the other samples were applied. For *S. aureus*, the inhibition zone of P(L-r-T)9 was very obvious, and the inhibition zone of P(P-r-T)1 could also be observed, while the inhibition zones of P(A-r-T)1, P(A-r-T)7 and P(L-r-T)1 needed to be observed very carefully, which may be related to the diffusion behavior of the samples on the agar plate. This also illustrates the limitation of this method, which is only suitable for samples with a strong antibacterial effect and easy diffusion on the agar plate.

Notably, increased hydrophobicity does not universally enhance antimicrobial activity in this system. While moderate amphiphilicity is sufficient for effective activity against *S. aureus*, overcoming the outer membrane barrier of *E. coli* requires a substantially higher hydrophilic and cationic content. This observation highlights the crucial role that the fundamental differences in the cell membrane structure of Gram-positive and Gram-negative bacteria play in determining the antimicrobial properties of polymers. For *S. aureus*, the absence of an outer membrane allows amphiphilic polymers with moderate hydrophobicity and cationic content to access and disrupt the cytoplasmic membrane relatively efficiently, leading to higher overall activity across much of the polymer library. In contrast, *E. coli* possesses a lipopolysaccharide-rich outer membrane that constitutes a significant permeability barrier. In this case, initial electrostatic interactions and charge accessibility dominate antimicrobial efficacy. Polymers with higher hydrophobic content may experience reduced aqueous dispersibility or partial self-association, limiting effective interaction with the negatively charged outer membrane. Only polymers with sufficiently high hydrophilic and cationic content remain well dispersed and exhibit enhanced activity against *E. coli*.

Cytotoxicity

Since there are many reports that cationic polymers can cause cytotoxicity by increasing the permeability of mammalian cell membranes, and the change in membrane permeability depends largely on the number of cationic charges on the polymer surface,[70,71] in order to evaluate the toxicity characteristics of such polymers in future applications, the cell viability of mouse fibroblasts (*L*929) after 24 h of exposure to the random copolymers was tested, and the results are shown in Fig. 3. The cell viability after 24 hours showed the same pattern for random copolymers composed of all cationic species in this study (Ala, Phe and Lys). In random polymers with lower cationic component content, no cytotoxicity was shown at a concentration of up to 5000 μg mL^{-1}, while the cytotoxicity gradually increased with the increase of cationic component content. Similar results have been reported in the literature previously.[40,47] Polymers with higher cationic content contain more protonated units, which catalyze the acid hydrolysis of ester bonds in the phospholipid bilayer of the cell membrane to form single-chain lipids and fatty acids. Then, the single-chain lipids will quickly destroy the stability of the membrane and cause cytotoxicity.[72,73] For random copolymers with Ala and Phe as cations, among the tested polymers, only the polymer with a cationic content of 90% showed certain cytotoxicity at concentrations of 5000 and 2500 μg mL^{-1}, respectively. It is worth mentioning that for the P(P-r-T)9 sample, the cell viability at a concentration of 2500 μg mL^{-1} was just 50%. For random copolymers with Lys as the cation, copolymers with more than 50% cationic components began to show cytotoxicity at a concentration of 5000 μg mL^{-1}, while cytotoxicity was reduced at 2500 μg mL^{-1}, and cell viability remained above 50%.

Selectivity to bacteria over mammalian cells

To examine the selective activity of random copolymers to bacterial cells over mammalian cells, we determined the IC50/MIC ratio as a selectivity measure (Table 3). In general, copolymers with Ala and Phe as cationic components have weak antibacterial activity against Gram-negative bacteria *E. coli* (MIC ≥ 2500 μg mL^{-1}), and their selectivity indexes for *E. coli* are very small (≤0.5), indicating that these polymers have no selectivity

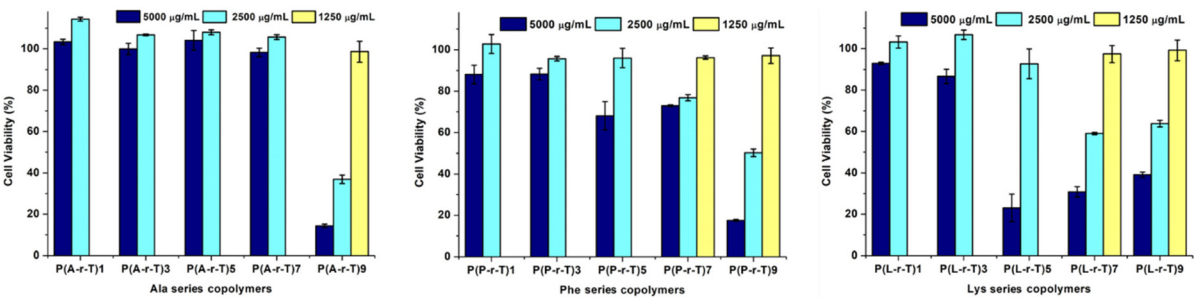

Fig. 3 The cytotoxicity of random copolymers with different cationic monomers and monomer feed ratios on cultured mouse fibroblasts (*L*929) after 24 h of incubation.

Open Access Article. Published on 22 apríl 2026. Downloaded on 03.06.2026 13:44:47.
This article is licensed under a Creative Commons Attribution 3.0 Unported Licence.

Table 3 Antimicrobial activity (MIC) and cytotoxicity (IC_{50}) of random copolymers with varying cationic monomers and monomer feed ratios

Random copolymers	MIC (μg mL^{-1})		IC_{50} [a] (μg mL^{-1})	Selectivity[b]	
	E. coli (ATCC 25922)	*S. aureus* (ATCC 6538)	*L*929	*E. coli* (ATCC 25922)	*S. aureus* (ATCC 6538)
P(A-r-T)1	>5000	500	>5000	—	>10
P(A-r-T)3	>5000	2000	>5000	—	>2.5
P(A-r-T)5	>5000	2000	>5000	—	>2.5
P(A-r-T)7	>5000	500	>5000	—	>10
P(A-r-T)9	2500	>2000	1250	0.5	<0.625
P(P-r-T)1	>5000	250	>5000	—	>20
P(P-r-T)3	>5000	2000	>5000	—	>2.5
P(P-r-T)5	>5000	2000	>5000	—	>2.5
P(P-r-T)7	>5000	2000	>5000	—	>2.5
P(P-r-T)9	5000	1000	2500	0.5	2.5
P(L-r-T)1	>5000	500	>5000	—	>10
P(L-r-T)3	>5000	1000	>5000	—	>5
P(L-r-T)5	1000	1000	2500	2.5	2.5
P(L-r-T)7	250	2000	2500	10	1.25
P(L-r-T)9	125	500	2500	20	5

[a] Concentration for a 50% reduction in cell viability. [b] Selectivity was calculated as IC_{50}/MIC.

for *E. coli* compared to animal cells. However, copolymers with Lys as the cationic component have obvious selectivity for *E. coli* over animal cells, which increases with the increase of the content of the cationic component. The selectivity coefficient increases from 2.5 for P(L-r-T)5 to 20 for P(L-r-T)9. For Gram-positive bacteria *S. aureus*, only P(A-r-T)9 and P(L-r-T)7 showed low or no selectivity among the tested polymers. The other samples showed certain selectivity; in particular, when the content of cationic components was small (10%), their selectivity was larger than 10 and the selectivity of Phe (with a hydrophobic benzene ring on the side chain) series polymers of the cationic component was larger than 20. It is worth mentioning that P(L-r-T)9 showed certain selectivity for both *E. coli* and *S. aureus* over *L*929 cells, with values of 20 and 5, respectively, indicating the possibility that it can be used to treat bacterial infections. Therefore, the subsequent antibacterial mechanism research was carried out using P(L-r-T)9.

Bacterial membrane integrity assay

Several researchers have proposed that the bactericidal mechanism of these amphiphilic antimicrobial agents involves an initial electrostatic interaction between the cationic components and the microbial cell membrane. This is followed by the insertion of hydrophobic groups, which disrupts membrane permeability, leading to a breakdown of transmembrane potential and leakage of intracellular contents, ultimately resulting in cell death.[65–67] To further investigate the said mechanism, bacterial viability was assessed using the Thermo Fisher Scientific LIVE/DEAD BacLight Kit to evaluate the integrity of bacterial cell membranes following treatment with the polymer P(L-r-T)9. This kit includes two dyes: green-fluorescent SYTO 9, which labels all bacterial cells in the sample, including those with intact and damaged membranes, and red-fluorescent propidium iodide (PI), which selectively penetrates only bacteria with compromised membranes.

In the control group, *E. coli* and *S. aureus* cells not treated with the polymer P(L-r-T)9 exhibited strong green fluorescence with no red fluorescence, indicating that all bacteria were alive with intact cell membranes (Fig. 4a-I, a-II, a-III, d-I, d-II, and d-III). In contrast, cells exposed to a 1MIC of the polymer solution for 4 hours showed reduced green fluorescence along with some red fluorescence signals, suggesting partial membrane damage; however, a substantial number of bacteria remained viable at this concentration (Fig. 4b-I, b-II, b-III, e-I, e-II, and e-III). At the higher concentration of 4MIC, the red fluorescence became more prominent, indicating extensive membrane damage and bacterial cell death, although some cells still survived (Fig. 4c-I, c-II, c-III, f-I, f-II, and f-III). These observations suggest that the polymer exerts bactericidal activity by disrupting bacterial cell membranes, which was further confirmed with SEM.

SEM can be employed to analyze the antimicrobial effects of synthetic polymers by observing characteristic morphological changes induced on bacterial membrane surfaces (Fig. 5). Untreated *E. coli* and *S. aureus* control cells exhibited bright, smooth, and undamaged membrane surfaces, as shown in the SEM micrographs (Fig. 5a-I and b-I). However, after treatment with P(L-r-T)9 at a concentration equal to MIC for 4 hours, noticeable alterations were observed. The surface of *E. coli* showed distinct depressions and the presence of particulate structures, while the membrane of *S. aureus* appeared rough and wrinkled and featured some vesicle formation, with even visible membrane disruptions in some cases. At a higher concentration of 4MIC for 4 hours, the membranes of both *E. coli* and *S. aureus* exhibited widespread damage and rupturing, resulting in collapsed cells.

In summary, these observations indicate that P(L-r-T)9 induces significant characteristic changes in the bacterial membrane surfaces, as evident from the SEM and live/dead staining. This leads to membrane rupture and the leakage of intracellular contents, ultimately causing bacterial cell death.

 This journal is © The Royal Society of Chemistry 2026

Open Access Article. Published on 22 aprel 2026. Downloaded on 03.06.2026 13:44:47.
This article is licensed under a Creative Commons Attribution 3.0 Unported Licence.

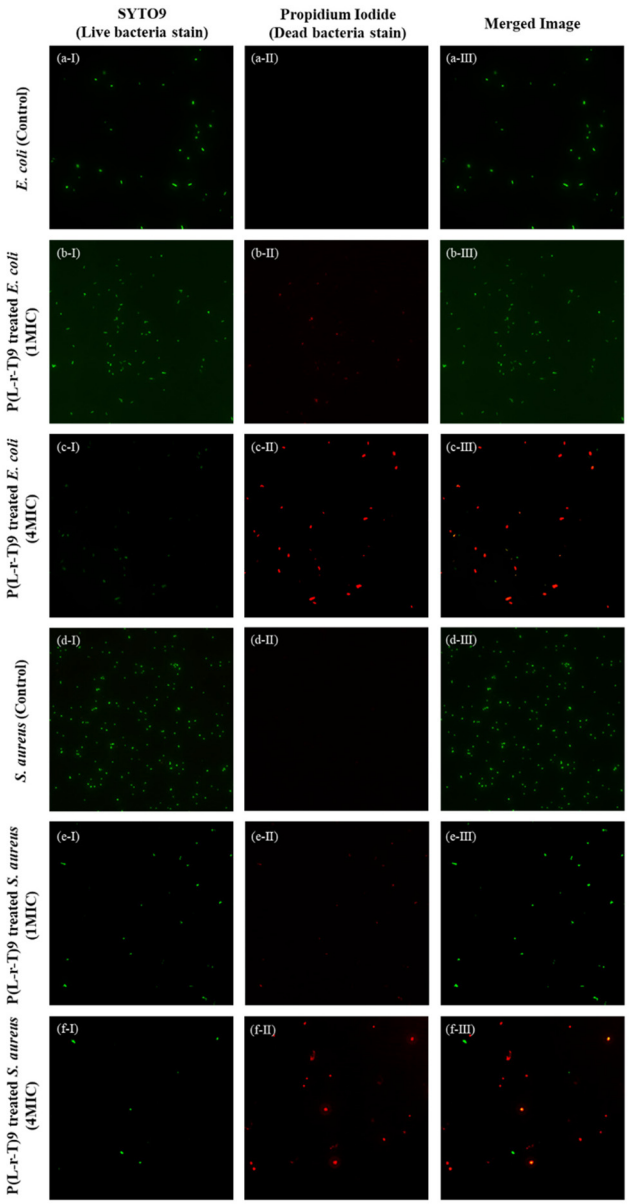

Fig. 4 Confocal laser scanning microscopy (CLSM) images of *E. coli* (from a-I to c-III) and *S. aureus* (from d-I to f-III) treated with P(L-r-T)9 at different concentrations (MIC and 4× MIC) for 4 h. (Green dots indicate live cells with an intact membrane, while red dots indicate dead cells with a compromised membrane; all images were taken at 40× magnification.)

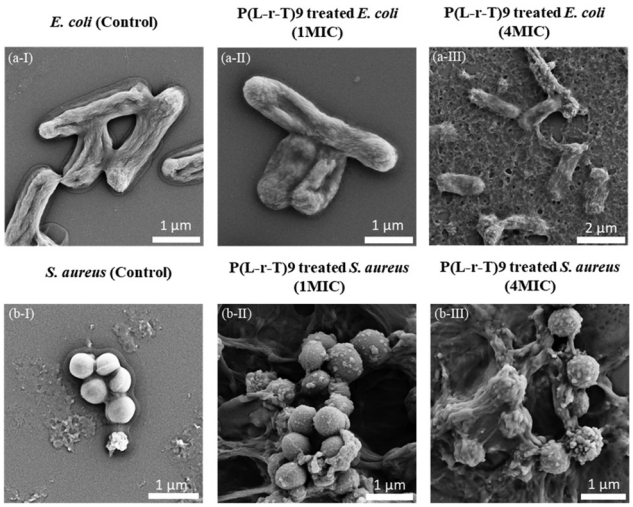

Fig. 5 SEM images of *E. coli* (from a-I to a-III) and *S. aureus* (from b-I to b-III) treated with P(L-r-T)9 at different concentrations (MIC and 4× MIC) for 4 h.

To further support the cell membrane breaking mechanism, a study of the interaction of the most active polymers, P(L-r-T)7 and P(L-r-T)9, with *E. coli* : PC vesicles was investigated using a calcein leakage experiment as described in the Materials and methods. Both polymers, P(L-r-T)7 and P(L-r-T)9, induced a concentration-dependent increase in calcein leakage (Fig. 6), indicating their ability to permeabilize the lipid bilayer and promote pore formation or membrane destabilization. However, their leakage profiles differed in magnitude and threshold of activity.

For P(L-r-T)7, the leakage activity progressively increased with concentration, reaching a maximum of 42% at 250 μg mL^{-1}. Notably, this concentration corresponds to the previously determined minimum inhibitory concentration (MIC) for this polymer, suggesting that membrane permeabilization may be directly linked to its antibacterial efficacy.

In contrast, P(L-r-T)9 showed significant leakage (44%) already at 60 μg mL^{-1}, below its MIC of 250 μg mL^{-1}. At 125 and 250 μg mL^{-1}, the leakage values remained similar (45% and 43%, respectively), indicating an early saturation of membrane-disruptive activity. This earlier onset of leakage may reflect a more specific or efficient interaction of P(L-r-T)9 with the lipid membrane compared to P(L-r-T)7. Interestingly, at concentrations above 250 μg mL^{-1}, both polymers showed a plateau or slight decrease in leakage activity. This non-linear trend suggests that optimal membrane interaction occurs at intermediate concentrations. Several mechanisms may underlie the reduced leakage at higher polymer doses, including polymer aggregation, limiting effective interaction with the bilayer; membrane rigidification, leading to stabilization rather than disruption; and direct interaction with calcein, potentially quenching fluorescence without additional leakage. Further investigation of this phenomenon is outside the scope of this work but may represent a follow-up study.

Overall, these results confirm that both polymers can disrupt lipid membranes in a concentration-dependent manner, with P(L-r-T)9 displaying earlier and more potent activity, possibly due to its enhanced membrane targeting properties. In contrast, P(L-r-T)7 exhibits its maximum leakage activity at 250 μg mL^{-1}, which coincides with its MIC, suggesting a direct correlation between membrane permeabilization and antimicrobial efficacy for this polymer.

Open Access Article. Published on 22 aprel 2026. Downloaded on 03.06.2026 13:44:47.
This article is licensed under a Creative Commons Attribution 3.0 Unported Licence.

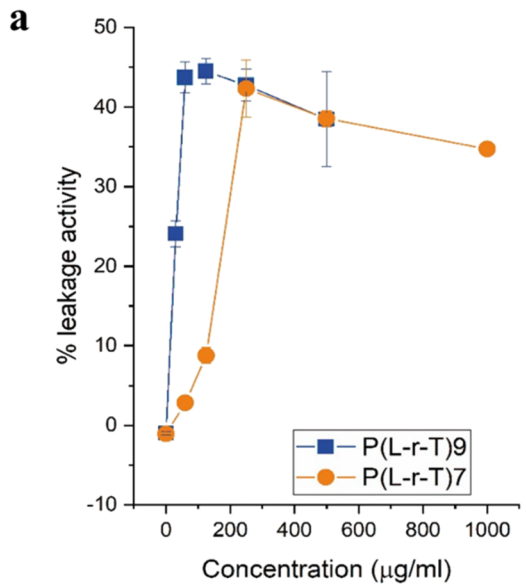

b

Polymer concentration (μg/mL)	P(L-r-T)9 (% leakage activity)	P(L-r-T)7 (% leakage activity)
0	-0.99±0.2	-1±0.2
31	24±1.6	not calculated
60	44±1.9	3±0.4
125	45±1.6	9±1.0
250	43±1.9	42±3.5
500	38±5.9	39±1.0
1000	not calculated	35±0.3

Fig. 6 (a) Calcein leakage activity of P(L-r-T)7 and P(L-r-T)9 as a function of polymer concentration. Large unilamellar vesicles (LUVs) composed of *E. coli* polar lipids and egg PC (3 : 1 molar ratio) were incubated with increasing concentrations of polymer (0–1000 μg mL^{-1}). Leakage was quantified as a percentage of total calcein release induced by Triton X-100. Data represent mean ± SD (n = 3). (b) Summary table of leakage values at different polymer concentrations for P(L-r-T)7 and P(L-r-T)9.

4. Conclusions

In summary, we successfully synthesized a library of 15 statistical amphiphilic random copolymers by using bio-based monomers, utilizing amino acids with different side chains (as cationic components) and tetrahydrogeraniol (as the hydrophobic component) as starting materials, turning them into methacrylates, and employing RAFT polymerization. These copolymers were screened against Gram-negative *E. coli* and Gram-positive *S. aureus*, as well as mouse fibroblast cells (*L*929), to evaluate their antimicrobial activity and cytotoxicity. We systematically examined the impact of the monomer ratio and the type of amino acid side chain (Ala, methyl; Phe, aromatic; Lys, cationic) on both antimicrobial activity and cytotoxicity. The results demonstrated that for *E. coli*, only the copolymers with the highest cationic content (up to 90%) from Ala and Phe exhibited antimicrobial activity. In contrast, the random copolymers composed of Lys showed gradually enhanced antimicrobial activity as the cationic content increased. For *E. coli*, there seems to be a direct correlation between water solubility and antimicrobial activity, but not for *S. aureus*. In this case, the balance between cationic components and hydrophobic chains influenced the MIC, with antimicrobial activity first decreasing and then increasing as the hydrophobic chain content decreased, with P(A-r-T)9 being the only outlier. In general, low solubility and polymer aggregation may be limiting factors in antimicrobial activity. Cytotoxicity also increased with higher cationic content. Among all the copolymers, P(L-r-T)9 exhibited notable antimicrobial activity against both *E. coli* and *S. aureus*, while demonstrating optimal selectivity for mammalian cells, and it is therefore the best candidate for practical applications. Live/dead staining and SEM results confirmed that its antimicrobial effect was mediated by disruption of the bacterial cell membrane. Consistently, calcein leakage assays in model liposomes composed of *E. coli* polar lipids and phosphatidylcholine (3 : 1) revealed that P(L-r-T)9 induces significant membrane permeabilization already at concentrations below its MIC, supporting a mechanism of action based on membrane destabilization and subsequent bacterial cell lysis. These findings provide valuable insights for the design and synthesis of more sustainable and effective antimicrobial amphiphilic polymers with strong biocompatibility.

Conflicts of interest

There are no conflicts to declare.

Data availability

Data for this article, including GPC, NMR, SEM, cytotoxicity, and dead cell staining, are available at Figshare at https://doi.org/10.6084/m9.figshare.31852735.

Supplementary information (SI): experimental section and characterization details; supplementary synthetic routes of amphiphilic antimicrobial random copolymers; ^{1}H and ^{13}C NMR spectra and analyses; and SEC and inhibition zone test results of polymers. See DOI: https://doi.org/10.1039/d6py00298f.

This journal is © The Royal Society of Chemistry 2026

Open Access Article. Published on 22 aprel 2026. Downloaded on 03.06.2026 13:44:47.
This article is licensed under a Creative Commons Attribution 3.0 Unported Licence.

Acknowledgements

The first author of this work was financially supported by the China Scholarship Council (CSC) under Grant Number 202204910075. We thank the European Union's Horizon 2020 research and innovation program, under the Marie Skłodowska-Curie grant agreement BioInspireSensing No. 955643, for supporting the research of Caterina Presutti.

References

1 P. Sarmah, M. M. Dan, D. Adapa and T. Sarangi, *Electron. J. Biol.*, 2018, **14**, 50–58.
2 D. M. Brogan and E. Mossialos, *Global. Health*, 2016, **12**, 8.
3 M. Kumar, D. K. Sarma, S. Shubham, M. Kumawat, V. Verma, P. B. Nina, D. Jp, S. Kumar, B. Singh and R. R. Tiwari, *Front. Microbiol.*, 2021, **12**, 609459.
4 S. Shahzadi, N. Zafar and R. Sharif, in *Bacterial Pathogenesis and Antibacterial Control*, Intechopen, London, 2018, 51, DOI: 10.5772/intechopen.72526.
5 R. Rawashdeh and Y. Haik, *Dyn. Biochem. Process Biotechnol. Mol. Biol.*, 2009, **3**, 12–20.
6 Y. Yan, Y. Li, Z. Zhang, X. Wang, Y. Niu, S. Zhang, W. Xu and C. Ren, *Colloids Surf., B*, 2021, **202**, 111682.
7 J. K. Boparai and P. K. Sharma, *Protein Pept. Lett.*, 2020, **27**, 4–16.
8 S. Duan, R. Wu, Y. Xiong, H. Ren, C. Lei, Y. Zhao, X. Zhang and F. Xu, *Prog. Mater. Sci.*, 2022, **125**, 100887.
9 K. Huang, C. Yang, S. Huang, C. Chen, Y. Lu and Y. Lin, *Int. J. Mol. Sci.*, 2016, **17**, 1578.
10 L. Timofeeva and N. Kleshcheva, *Appl. Microbiol. Biotechnol.*, 2011, **89**, 475–492.
11 J. Chen, F. Wang, Q. Liu and J. Du, *Chem. Commun.*, 2014, **50**, 14482–14493.
12 T. I. Shabatina, O. I. Vernaya and M. Y. Melnikov, *Molecules*, 2023, **28**, 1603.
13 U. Patel and E. C. Hunt, *J. Nanotheranostics*, 2023, **4**, 429–462.
14 M. Manoswini, D. Bhattacharya, P. Sen, N. Ganguly and P. S. Mohanty, *Adv. Nat. Sci.: Nanosci. Nanotechnol.*, 2021, **12**, 025003.
15 L. J. Zhang and R. L. Gallo, *Curr. Biol.*, 2016, **26**, R14–R19.
16 W. C. Wimley, *ACS Chem. Biol.*, 2010, **5**, 905–917.
17 K. Matsuzaki, *Biochim. Biophys. Acta, Biomembr.*, 1999, **1462**, 1–10.
18 Y. Q. Xiong, K. Mukhopadhyay, M. R. Yeaman, J. Adler-Moore and A. S. Bayer, *Antimicrob. Agents Chemother.*, 2005, **49**, 3114–3121.
19 N. Malanovic and K. Lohner, *Pharmaceuticals*, 2016, **9**, 59.
20 V. I. Band and D. S. Weiss, *Antibiotics*, 2015, **4**, 18–41.
21 A. H. Benfield and S. T. Henriques, *Front. Med. Technol.*, 2020, **2**, 2020.
22 G. Moad, E. Rizzardo and S. H. Thang, *Chem.– Asian J.*, 2013, **8**, 1634–1644.
23 F. L. Hatton, *Polym. Chem.*, 2020, **11**, 220–229.
24 N. P. Truong, G. R. Jones, K. G. Bradford, D. Konkolewicz and A. Anastasaki, *Nat. Rev. Chem.*, 2021, **5**, 859–869.
25 N. Corrigan, K. Jung, G. Moad, C. J. Hawker, K. Matyjaszewski and C. Boyer, *Prog. Polym. Sci.*, 2020, **111**, 101311.
26 D. S. Uppu, S. Samaddar, C. Ghosh, K. Paramanandham, B. R. Shome and J. Haldar, *Biomaterials*, 2016, **74**, 131–143.
27 K. E. Locock, T. D. Michl, J. D. Valentin, K. Vasilev, J. D. Hayball, Y. Qu, A. Traven, H. J. Griesser, L. Meagher and M. Haeussler, *Biomacromolecules*, 2013, **14**, 4021–4031.
28 K. Kuroda and W. F. DeGrado, *J. Am. Chem. Soc.*, 2005, **127**, 4128–4129.
29 K. Kuroda, G. A. Caputo and W. F. DeGrado, *Chem. – Eur. J.*, 2009, **15**, 1123–1133.
30 K. Lienkamp and G. N. Tew, *Chem. – Eur. J.*, 2009, **15**, 11784–11800.
31 K. Lienkamp, A. E. Madkour, A. Musante, C. F. Nelson, K. Nusslein and G. N. Tew, *J. Am. Chem. Soc.*, 2008, **130**, 9836–9843.
32 G. J. Gabriel, J. A. Maegerlein, C. F. Nelson, J. M. Dabkowski, T. Eren, K. Nüsslein and G. N. Tew, *Chem. – Eur. J.*, 2009, **15**, 433–439.
33 H. Takahashi, G. A. Caputo, S. Vemparala and K. Kuroda, *Bioconjugate Chem.*, 2017, **28**, 1340–1350.
34 K. Lienkamp, K. N. Kumar, A. Som, K. Nüsslein and G. N. Tew, *Chem. – Eur. J.*, 2009, **15**, 11710–11714.
35 J. Pachla, R. J. Kopiasz, G. Marek, W. Tomaszewski, A. Głogowska, K. Drężek, S. Kowalczyk, R. Podgórski, B. Butruk-Raszeja, T. Ciach, J. Mierzejewska, A. Plichta, E. Augustynowicz-Kopeć and D. Jańczewski, *Biomacromolecules*, 2023, **24**, 2237–2249.
36 Z. Cheng and P. Raffa, *Mater. Adv.*, 2025, **6**, 4939–4968.
37 P. Pham, S. Oliver, E. H. Wong and C. Boyer, *Polym. Chem.*, 2021, **12**, 5689–5703.
38 R. Namivandi-Zangeneh, R. J. Kwan, T.-K. Nguyen, J. Yeow, F. L. Byrne, S. H. Oehlers, E. H. Wong and C. Boyer, *Polym. Chem.*, 2018, **9**, 1735–1744.
39 R. Bhat, L. L. Foster, G. Rani, S. Vemparala and K. Kuroda, *RSC Adv.*, 2021, **11**, 22044–22056.
40 S. Schaefer, D. Melodia, C. Pracey, N. Corrigan, M. D. Lenardon and C. Boyer, *Biomacromolecules*, 2024, **25**, 871–889.
41 Y. Hu, J. Zhao, J. Zhang, Z. Zhu and J. Rao, *ACS Macro Lett.*, 2021, **10**, 990–995.
42 A. Tyagi and A. Mishra, *ACS Omega*, 2021, **6**, 34724–34735.
43 S. Hong, H. Takahashi, E. T. Nadres, H. Mortazavian, G. A. Caputo, J. G. Younger and K. Kuroda, *PLoS One*, 2017, **12**, e0169262.
44 P. T. Phuong, S. Oliver, J. He, E. H. H. Wong, R. T. Mathers and C. Boyer, *Biomacromolecules*, 2020, **21**, 5241–5255.
45 V. Sambhy, B. R. Peterson and A. Sen, *Angew. Chem., Int. Ed.*, 2008, **47**, 1250–1254.
46 I. Sovadinova, E. F. Palermo, M. Urban, P. Mpiga, G. A. Caputo and K. Kuroda, *Polymers*, 2011, **3**, 1512–1532.
47 E. F. Palermo and K. Kuroda, *Biomacromolecules*, 2009, **10**, 1416–1428.

Open Access Article. Published on 22 aprel 2026. Downloaded on 03.06.2026 13:44:47.
This article is licensed under a Creative Commons Attribution 3.0 Unported Licence.

48 Y. Oda, S. Kanaoka, T. Sato, S. Aoshima and K. J. B. Kuroda, *Biomacromolecules*, 2011, **12**, 3581–3591.
49 T. Maity, S. Paul and P. Y. De, *J. Macromol. Sci., Part A:Pure Appl. Chem.*, 2023, **60**, 2–17.
50 I. Mukherjee, A. Ghosh, P. Bhadury and P. De, *ACS Omega*, 2017, **2**, 1633–1644.
51 J. Zhu, H. Han, F. Li, X. Wang, J. Yu, C.-C. Chu and D. Wu, *J. Colloid Interface Sci.*, 2019, **540**, 634–646.
52 J. Koehbach and D. J. Craik, *Trends Pharmacol. Sci.*, 2019, **40**, 517–528.
53 S. Noppalit, A. Simula, N. Ballard, X. Callies, J. M. Asua and L. Billon, *Biomacromolecules*, 2019, **20**, 2241–2251.
54 J. Tan, Y. Zhao, J. L. Hedrick and Y. Yang, *Adv. Healthcare Mater.*, 2022, **11**, 2100482.
55 S. G. Roy and P. De, *Polymer*, 2014, **55**, 5425–5434.
56 L. M. Jost, J. M. Kirkwood and T. L. Whiteside, *J. Immunol. Methods*, 1992, **147**, 153–165.
57 D. A. Scudiero, R. H. Shoemaker, K. D. Paull, A. Monks, S. Tierney, T. H. Nofziger, M. J. Currens, D. Seniff and M. R. Boyd, *Cancer Res.*, 1988, **48**, 4827–4833.
58 M. A. Auty, G. E. Gardiner, S. J. McBrearty, E. O. O'Sullivan, D. M. Mulvihill, J. K. Collins, G. F. Fitzgerald, C. Stanton and R. P. Ross, *Appl. Environ. Microbiol.*, 2001, **67**, 420–425.
59 L. Boulos, M. Prévost, B. Barbeau, J. Coallier and R. Desjardins, *J. Microbiol. Methods*, 1999, **37**, 77–86.
60 M. J. Newman and T. H. Wilson, *J. Biol. Chem.*, 1980, **255**, 10583–10586.
61 E. F. Palermo, S. Vemparala and K. Kuroda, *Biomacromolecules*, 2012, **13**, 1632–1641.
62 S. C. Owen, D. P. Y. Chan and M. S. Shoichet, *Nano Today*, 2012, **7**, 53–65.
63 A. Jain, L. S. Duvvuri, S. Farah, N. Beyth, A. J. Domb and W. Khan, *Adv. Healthcare Mater.*, 2014, **3**, 1969–1985.
64 H. Takahashi, G. A. Caputo and K. Kuroda, *Biomater. Sci.*, 2021, **9**, 2758–2767.
65 R. F. Epand, B. P. Mowery, S. E. Lee, S. S. Stahl, R. I. Lehrer, S. H. Gellman and R. M. Epand, *J. Mol. Biol.*, 2008, **379**, 38–50.
66 H. Murata, R. R. Koepsel, K. Matyjaszewski and A. J. Russell, *Biomaterials*, 2007, **28**, 4870–4879.
67 J. Y. Huang, R. R. Koepsel, H. Murata, W. Wu, S. B. Lee, T. Kowalewski, A. J. Russell and K. Matyjaszewski, *Langmuir*, 2008, **24**, 6785–6795.
68 N. Kawabata and M. Nishiguchi, *Appl. Environ. Microbiol.*, 1988, **54**, 2532–2535.
69 P. Pham, S. Oliver and C. Boyer, *Macromol. Chem. Phys.*, 2023, **224**, 2200226.
70 S. Hong, P. R. Leroueil, E. K. Janus, J. L. Peters, M. M. Kober, M. T. Islam, B. G. Orr, J. R. Baker Jr. and M. M. Banaszak Holl, *Bioconjug. Chem.*, 2006, **17**, 728–734.
71 F. Unger, M. Wittmar and T. Kissel, *Biomaterials*, 2007, **28**, 1610–1619.
72 D. M. L. Morgan, V. L. Larvin and J. D. Pearson, *J. Cell Sci.*, 1989, **94**, 553–559.
73 D. M. L. Morgan, J. Clover and J. D. Pearson, *J. Cell Sci.*, 1988, **91**, 231–238.

This journal is © The Royal Society of Chemistry 2026